# Detailed study of a high-finesse planar waveguide for evanescent wave atomic mirrors

Quantum Semiclass. Opt. **8** (1996) 603–627. Printed in the UK

# Detailed study of a high-finesse planar waveguide for evanescent wave atomic mirrors

G Labeyrie, A Landragin, J Von Zanthier, R Kaiser, N Vansteenkiste, C Westbrook and A Aspect

Institut d'Optique, URA 14 du CNRS, BP 147, 91403 Orsay, France

Received 4 January 1996, in final form 8 February 1996

**Abstract.** We have realized a resonant waveguide structure which enhances the intensity of an evanescent wave at a dielectric–vacuum interface by more than three orders of magnitude. We present a simple theoretical model including the effect of the losses in the waveguide, which gives a good description of the observed behaviour of the structure. We experimentally determine the enhancement factor by analysing the resonance of the reflected light intensity. This characterization technique allows for an easy *in situ* monitoring of the enhancement, which is a key feature for the understanding of atomic mirror experiments.

## 1. Introduction

The use of the dipole force in an evanescent wave to reflect atoms was proposed in [1], and has received a great deal of experimental attention [2–12]. This is because such a device is a very promising way to make an atomic mirror, and our experience in optics leads us to expect that good mirrors will be important tools for atom optics. To be really useful it is important that the atomic mirror be 'coherent', i.e. that it preserve the coherence of the incident wave. Thus, random processes such as spontaneous emission must be avoided. One can show that, for a fixed incident velocity, the minimum probability of spontaneous emission during the bounce is inversely proportional to the laser intensity creating the evanescent wave [6, 10]. In all the experiments of [2–6], the spontaneous emission probability was equal to or greater than about 10% per atom per reflection. It is therefore important to increase the intensity of evanescent waves to obtain coherent atomic mirrors. A solution for reaching higher intensities is to enhance the evanescent wave using a passive resonant structure. Atomic mirrors based on this idea have been demonstrated, making use of both surface plasmons [7–9] and of a dielectric waveguide structure [10–13].

The waveguide used in [10] was described in a previous paper [14]. The principle of the enhancement was explained, and we showed that the main features of the structure could be qualitatively understood using an analogy with a Fabry–Perot cavity. We also introduced a method to evaluate the enhancement, based on the analysis of the reflected light. The treatment of the experimental data yielded a value of 130 for the enhancement factor, the ratio of the effective intensity $\epsilon_0 c E^2/2$ of the evanescent wave at the interface with and without the waveguide. In this first system, the influence of the losses was negligible.

In this paper, we describe an improved structure with an enhancement factor of 1650, a gain of more than one order of magnitude. With this structure we were able to reflect atoms with a spontaneous emission probability below 1% [11, 12]. Understanding the behaviour

1355-5111/96/030603+25$19.50  

of this highly resonant system requires a more detailed analysis than in the previous case. In particular, the losses have to be accounted for to calculate the enhancement. We will also use a Lorentzian approximation to derive some simple analytical expressions for the transmission and reflection coefficients of the structure as a function of the wavelength [15]. This provides a simple understanding of the influence of the various parameters of the structure and a straightforward way to estimate the enhancement, using the quantities characterizing the reflectivity curve. We have applied this method to our device placed in the conditions of the atomic mirror experiments (i.e. inside a UHV chamber). We measure the intensity of the light reflected by the structure as a function of the wavelength, and use the quantities characterizing this reflectivity curve to calculate the enhancement factor. This remote measurement technique permits easy *in situ* characterization of the resonance. It has enabled us to observe the evolution of the structure with time, a phenomenon that we attribute to a reversible pollution of the prism surface by rubidium atoms.

In section 2, we present the detailed analysis of the enhancement of evanescent waves using a dielectric waveguide structure. We describe in section 2.1 the structure of the multilayered system, and recall the simple analogy with a Fabry–Perot cavity which allows a qualitative understanding. We then introduce the notation used throughout the paper, and recall the results of the exact plane-wave treatment based on the Fresnel coefficients (section 2.2). In sections 2.3 and 2.4, we discuss the behaviour of the device in the 'low-coupling' regime, analogous to a high reflectivity input coupler in a Fabry–Perot, both without and with losses in the waveguide layer. Two different regimes appear, depending on the value of the losses with respect to the coupling. In section 2.5, we use the Lorentzian approximation to derive some simplified expressions for the transmission and reflection coefficients of the structure around resonance. Using these results, we show that the enhancement can be easily obtained through the analysis of the reflected light.

In section 3, we present experimental results obtained with the system described in this paper. The experimental set up, allowing for the *in situ* measurement of the reflectivity of the structure, is described in section 3.1. We then show how we analyse the experimental data (section 3.2). This analysis yields a value for the enhancement of the evanescent wave. We finally report, in section 3.3, on the time evolution of the resonance due to contamination by rubidium atoms.

## 2. Theory

### *2.1. Description of the system*

The waveguide structure under study is illustrated in figure 1. Two thin dielectric layers are evaporated onto a glass prism with a high index of refraction $n_1$. The first film, with a low index of refraction $n_2$ and a thickness $d_2$, acts as a gap layer between the prism and the second layer, characterized by a high index of refraction $n_3$ and a thickness $d_3$. This second layer, surrounded by two media of lower indices (the gap layer below and the vacuum above), acts as a single-mode waveguide at the operating wavelength ($\lambda = 780$ nm). The incident light is coupled inside the waveguide through the gap layer, making use of frustrated total internal reflection at the prism–gap interface.

To understand how this structure enhances the evanescent wave, we can use an analogy with a Fabry–Perot cavity. In this analogy, the gap corresponds to a coupling mirror, whose transmission is small in our case. The waveguide–vacuum interface, where the light is totally reflected, corresponds to the second mirror of the cavity, with a reflection coefficient equal to 1. We thus have a Fabry–Perot cavity of high finesse: for certain values of the incident

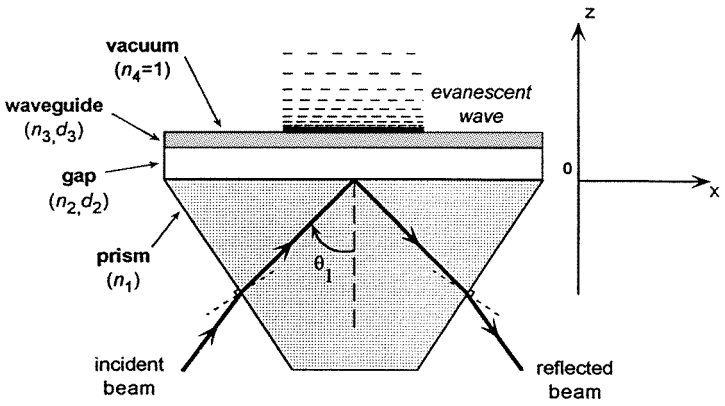


**Figure 1.** Resonant dielectric waveguide structure. The high-index waveguide ($TiO_2$, thickness $d_3 = 69.7$ nm, index of refraction $n_3 = 2.387$) is separated from the prism (LaSFN18, index of refraction $n_1 = 1.893$) by a low-index gap ($SiO_2$, thickness $d_2 = 700$ nm, index of refraction $n_2 = 1.49$). All indices are given for $\lambda = 780$ nm. The dielectric layers are deposited by ion-assisted deposition (IAD). The incident laser beam can be resonantly coupled to a waveguide mode, through the gap, by frustrated total internal reflection ('photon tunnelling'). This results in a large amplitude evanescent wave in the vacuum above the waveguide.

light parameters (e.g. the wavelength), the electric field amplitude inside the waveguide experiences a strong resonant build-up; by continuity, the evanescent wave amplitude in the vacuum above the waveguide is also enhanced.

### *2.2. Plane-wave description*

In the theoretical section, we consider an incident plane wave in the prism. The influence of the Gaussian profile of the laser beam will appear in the analysis of the experimental results. Therefore, the electric field in each medium will be described by the sum of two plane waves. We assume TE polarization for the incident plane wave, so all the electric fields in the problem are perpendicular to the plane of figure 1 ($x$–$z$ plane). The time dependence of the electric field is described by a term $\exp(-\mathrm{i}\omega t)$. The complex amplitude of the electric field of a plane wave in medium $j$ is

$$E_j(x,z) = A_j \exp[\mathrm{i}(k_{xj}x + k_{zj}z)] \tag{1}$$

where $k_{xj}$ and $k_{zj}$ are the components of the wave vector along the $x$ and $z$ axis, respectively.

The total electric field in medium $j$ can be written as the sum of an incident (upward propagating) wave and a reflected (downward propagating) wave:

$$\begin{aligned} E_j(x,z) &= E_j^{\mathrm{inc}}(x,z) + (1-\delta_{j4})E_j^r(x,z) \\ &= A_j^{\mathrm{inc}} \exp[\mathrm{i}(k_{xj}x + k_{zj}z)] + (1-\delta_{j4})A_j^{\mathrm{inc}} \exp[\mathrm{i}(k_{xj}x - k_{zj}z)]. \end{aligned} \tag{2}$$

The Kronecker symbol $\delta_{j4}$ accounts for the fact that there is no reflected wave in medium 4, which is semi-infinite. The components $k_{xj}$ and $k_{zj}$ of the wave vector in medium $j$ are linked by the relation

$$k_{xj}^2 + k_{zj}^2 = n_j^2 \frac{\omega^2}{c^2}\,. \tag{3}$$

Because of the Snell–Descartes laws, all the $k_{xj}$ components are equal:

$$k_{xj} = \frac{\omega}{c} n_1 \sin\theta_1 = k_x \tag{4}$$

where $\theta_1$ denotes the incidence angle in the prism. To obtain total internal reflection at the prism–gap interface, we operate with $\theta_1$ satisfying $\sin\theta_1 > n_2/n_1$. According to the values given in figure 1, we have: $n_3 > n_1 > n_2 > n_4$; therefore, the electromagnetic waves are propagative along the $z$-axis in the prism ($j = 1$) and the waveguide ($j = 3$), and evanescent in the gap ($j = 2$) and vacuum ($j = 4$). Thus we write the electric field amplitudes in the prism and the waveguide:

$$E_j(x, z) = \left(A_j^{\text{inc}} \exp\left(k_{zj}z\right) + A_j^r \exp\left(-k_{zj}z\right)\right) \exp\left(\mathrm{i}k_x x\right) \tag{5}$$

with

$$k_{zj} = \sqrt{n_j^2 \frac{\omega^2}{c^2} - k_x^2} \qquad \text{for} \quad j = 1 \text{ and } 3\,. \tag{6}$$

Similarly, in the gap and the vacuum we have

$$E_j(x, z) = \left(A_j^{\text{inc}} \exp(-\kappa_j z) + (1 - \delta_{j4}) A_j^r \exp(\kappa_j z)\right) \exp\left(\mathrm{i}k_x x\right) \tag{7}$$

with

$$\kappa_j = \sqrt{k_x^2 - n_j^2 \frac{\omega^2}{c^2}} \qquad \text{for} \quad j = 2 \text{ and } 4\,. \tag{8}$$

The amplitude Fresnel coefficients for reflection and transmission at the interface $i$–$j$ are denoted by $r_{ij}$ and $t_{ij}$, respectively. In a very general way, we can write

$$r_{ij} = |r_{ij}| \exp(-2\mathrm{i}\Phi_{ij})\,. \tag{9}$$

In our particular situation, there is total internal reflection at the prism–gap interface, as well as at the waveguide–gap and waveguide–vacuum interfaces. Thus, in the absence of losses, one has $|r_{12}| = 1$ and $|r_{3j}| = 1$, for $j = 2$ and 4. When losses are taken into account in the waveguide, one has $|r_{3j}| < 1$ [16]. It is also convenient to introduce a generalized Fresnel coefficient describing the amplitude reflection of the waveguide layer, surrounded by the two semi-infinite media 2 and 4 [16]:

$$r_{234} = \frac{r_{23} + r_{34} \exp\left(-2\mathrm{i}k_{z3}d_3\right)}{1 + r_{23}r_{34} \exp\left(-2\mathrm{i}k_{z3}d_3\right)} = |r_{234}| \exp\left(-2\mathrm{i}\Phi_{234}\right). \tag{10}$$

Using the same approach, we can similarly define the generalized Fresnel coefficients for our structure, $t_{1234}$ and $r_{1234}$:

$$t_{1234} = \frac{E_4\left(x, z = d_2 + d_3\right)}{E_1^{\text{inc}}\left(x, z = 0\right)} \equiv t_{14} \tag{11}$$

and

$$r_{1234} = \frac{E_1^r\left(x, z = 0\right)}{E_1^{\text{inc}}\left(x, z = 0\right)} \equiv r_{14}\,. \tag{12}$$

In expressions (11) and (12), we introduced the abbreviated notation $t_{14}$ and $r_{14}$ for the sake of simplicity; however, the reader should keep in mind that these quantities are composite terms involving the Fresnel coefficient at the various interfaces and the indices of refraction and thicknesses of the dielectric layers.

The term $|t_{14}|^2$, which we will refer to as the transmission factor in the rest of this paper, is the most important quantity in our problem, since it measures the performance of the device. More precisely, the enhancement is proportional to $|t_{14}|^2$. However, $|t_{14}|^2$ is not directly measurable in our experiment, since it is difficult to have access to the electric field amplitude in the evanescent wave at the dielectric–vacuum interface [17]. Instead, we will extract this information from the analysis of the reflection coefficient $|r_{14}|^2$, which is easier to measure in our experiment.

### *2.3. Loss-free waveguide*

Writing the continuity of the electric field at the various interfaces, it is possible to obtain an exact expression of the amplitude transmission and reflection coefficients $t_{14}$ and $r_{14}$, as a function of the Fresnel coefficients $r_{ij}$ and $t_{ij}$ and of the thicknesses and indices of the layers. The amplitude transmission factor can be written as [18]

$$t_{14} = \frac{t_{12}t_{23}t_{34}\exp(\mathrm{i}k_{z3}d_3)}{F\exp(\kappa_2 d_2) + G\exp(-\kappa_2 d_2)} \tag{13}$$

with

$$F = 1 - r_{34}r_{32}\exp(2\mathrm{i}k_{z3}d_3) \tag{14}$$

$$G = r_{12}r_{23} - r_{34}r_{21}\exp(2\mathrm{i}k_{z3}d_3)\,. \tag{15}$$

The amplitude reflection coefficient is given by

$$r_{14} = \frac{r_{12} + r_{234}\exp(-2\kappa_2 d_2)}{1 + r_{12}r_{234}\exp(-2\kappa_2 d_2)} \tag{16}$$

where the expression of $r_{234}$ is given in (10).

Since we are interested in strongly resonant systems, we will restrict our discussion to the case of a thick gap layer, so that

$$\exp(-2\kappa_2 d_2) \ll 1\,. \tag{17}$$

We refer to this situation, where the fraction of an incident plane wave intensity transmitted through the gap layer is small, as the 'low-coupling' regime. For our parameters (see figure 1), one finds: $\kappa_2 \approx 4/\lambda$ and $\exp(-2\kappa_2 d_2) \simeq 4 \times 10^{-4}$.

Using expressions (13) and (16), it is possible to plot the transmission and reflection coefficients $|t_{14}|^2$ and $|r_{14}|^2$ as a function of the wavelength $\lambda$. Since we have assumed in this section that the system is free from losses, all the incident light is reflected by the prism and it is not surprising to find the reflection coefficient $|r_{14}|^2$ equal to 1 for all wavelengths. In figure 2, we have plotted the transmission factor $|t_{14}|^2$ as a function of $\lambda$ for two different values of the gap thickness $d_2$. We see that the transmission factor exhibits a resonant behaviour, i.e. $|t_{14}|^2$ strongly increases for the resonance wavelength. Furthermore, the on-resonance value of the transmission factor, which we denote by $|t_{14}|^2_{\mathrm{res}}$, strongly increases with the gap thickness, while the width of the resonance curve decreases.

This can be understood with expression (13). We see that, usually, $|t_{14}|^2$ is small ($\exp(\kappa_2 d_2) \gg 1$), but if $F$ is zero, $|t_{14}|^2$ can become very large. From expression (14), this occurs when

$$r_{34}r_{32}\exp(2\mathrm{i}k_{z3}d_3) = 1\,. \tag{18}$$

Using the notation introduced in (9), and in the absence of losses, we can write (18) in the form

$$\Psi = 2k_{z3}d_3 - 2\Phi_{32} - 2\Phi_{34} = 2m\pi \tag{19}$$

where $m$ is an integer. Equation (19) corresponds to the resonance condition for the waveguide layer surrounded by two semi-infinite media (the vacuum above and a medium with the index of refraction $n_2$ below), i.e. when the prism is at an infinite distance from the waveguide ($d_2 = \infty$). Note that the phase shift $\Psi$ given in expression (19) depends, for a given structure (i.e. fixed thicknesses and indices), only on the wavelength $\lambda$ and the incidence angle $\theta_1$, so that both quantities can be adjusted to excite a mode. Because the waveguide is very thin (see figure 1), the only mode allowed for $\lambda = 780$ nm is the zeroth-order mode ($m = 0$) for TE polarization.

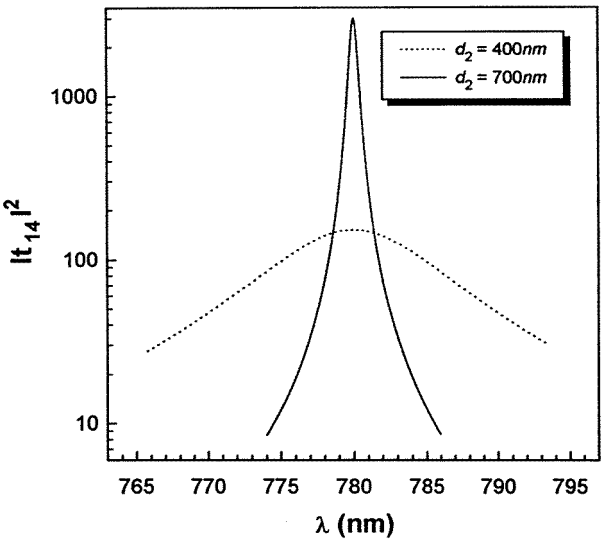


**Figure 2.** Resonant behaviour of the transmission factor $|t_{14}|^2$ in the loss-free case, as a function of the wavelength, for two values of the gap thickness $d_2$. $t_{14}$ is the ratio of the electric field amplitudes in the evanescent wave and in the prism, as defined in equation (11). The resonance is more pronounced when the gap is thicker.

In fact, due to the finite thickness of the gap $d_2$, the maximum of the transmission factor $|t_{14}|^2$ does not exactly correspond to the zero of $F$, i.e. the resonance for the complete structure occurs for conditions slightly different from those of the 'uncoupled' waveguide ($d_2 = \infty$). This effect, however, is small since we consider only large gap thicknesses, and can be neglected in the present discussion. This amounts to taking $F = 0$ in expression (13), and we thus obtain

$$|t_{14}|^2_{\text{res}} \propto \exp(2\kappa_2 d_2) . \tag{20}$$

This is an important feature of our system: although the off-resonance transmission factor drops exponentially to zero when the gap thickness $d_2$ increases (see expression (13)), the on-resonance transmission factor $|t_{14}|^2_{\text{res}}$, in contrast, increases exponentially with $d_2$. This clearly appears when comparing the two curves in figure 2.

Note that all the features described above can be understood using the Fabry–Perot analogy introduced in section 2.1. When the transmission of the coupling mirror decreases, the finesse of the cavity increases, in the absence of losses. The build-up of the electric field inside the cavity is proportional to the finesse, so we expect the enhancement of the evanescent wave to increase exponentially with the gap thickness. The improvement of the finesse of the cavity when $d_2$ increases also results in the narrowing of the resonance peak.

### *2.4. Lossy waveguide*

So far we have considered a lossless structure. Our system, however, is subject to several loss mechanisms: absorption, bulk and interface scattering. Our observations show that the reflection coefficient $|r_{14}|^2$ decreases by at least 20% on resonance (see figure 8). On the other hand, when the laser is far from resonance, and when corrected for the Fresnel coefficients of the input and output faces of the prism, $|r_{14}|^2$ is very close to unity. This means that, on resonance, most of our loss comes from the waveguide, where the

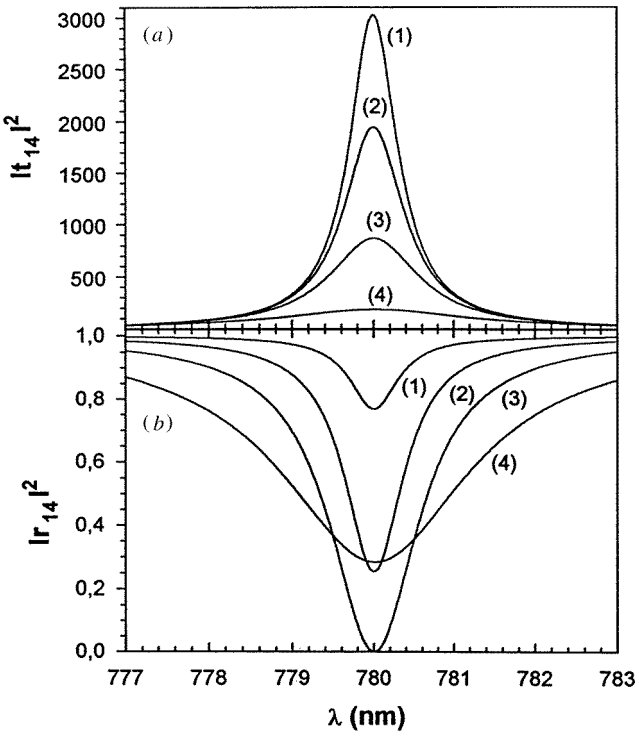


**Figure 3.** (*a*) Transmission factor $|t_{14}|^2$ and (*b*) reflection coefficient $|r_{14}|^2$ as a function of the wavelength in the presence of losses. The gap thickness is fixed ($d_2 = 700$ nm) and the losses, included through an imaginary part of the index of refraction of the waveguide, are varied. (1) $n_3'' = 2 \times 10^{-5}$; (2) $n_3'' = 10^{-4}$; (3) $n_3'' = 3 \times 10^{-4}$; (4) $n_3'' = 10^{-3}$.

electromagnetic energy density is very high. Thus, in our simple model, we only take into account the losses in the waveguide, by adding an imaginary part to the refractive index of this layer:

$$n_3 = n_3' + \mathrm{i}n_3''. \tag{21}$$

We assume here that $n_3''$ accounts not only for the losses occurring in the bulk of the waveguide layer, but also for those due to scattering at the waveguide–gap and waveguide–vacuum interfaces.

The amplitude transmission and reflection coefficients $t_{14}$ and $r_{14}$ can still be calculated using expressions (13) and (16), where the index of refraction of the waveguide has been replaced by expression (21). In figure 3, we have plotted the transmission and reflection coefficients $|t_{14}|^2$ and $|r_{14}|^2$ as a function of the wavelength, for different values of the losses and a fixed gap thickness $d_2 = 700$ nm. We see in figure 3(*a*) that, as $n_3''$ increases, the transmission curve broadens while the peak value $|t_{14}|^2_{\mathrm{res}}$ decreases rapidly. In figure 3(*b*), we see that due to the losses, $|r_{14}|^2$ is no longer equal to 1 for all wavelengths, but presents a marked dip on resonance. The characteristic parameters of this curve will allow us to extract the information on $|t_{14}|^2_{\mathrm{res}}$. Starting from small values of $n_3''$, the on-resonance reflection coefficient $|r_{14}|^2_{\mathrm{res}}$ first decreases with $n_3''$, reaches zero for $n_3'' \simeq 3 \times 10^{-4}$, and then increases.

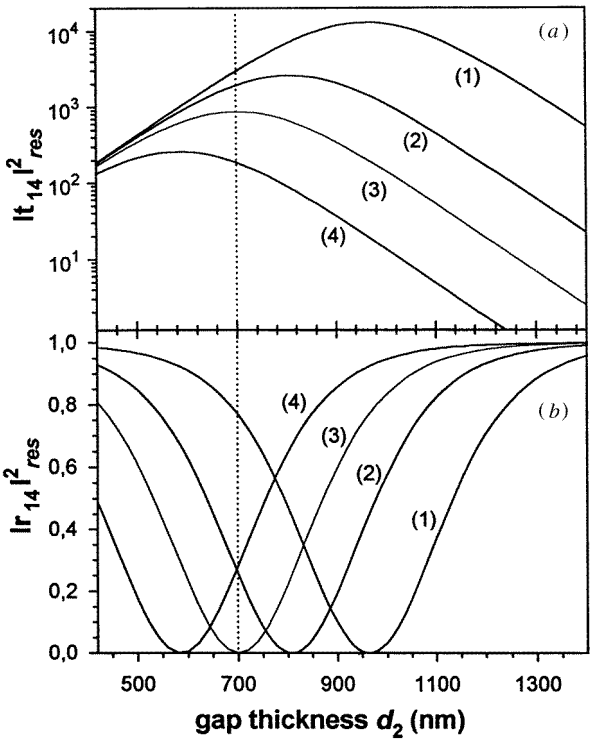


**Figure 4.** (*a*) On-resonance transmission factor $|t_{14}|^2_{\rm res}$ and (*b*) reflection coefficient $|r_{14}|^2_{\rm res}$ as a function of the gap thickness $d_2$, for different values of the losses. The values of $n_3''$ are the same as in figure 3. (1) $n_3'' = 2 \times 10^{-5}$; (2) $n_3'' = 10^{-4}$; (3) $n_3'' = 3 \times 10^{-4}$; (4) $n_3'' = 10^{-3}$. The dotted vertical line at $d_2 = 700$ nm corresponds to the conditions of figure 3.

We are also interested in the influence of the gap thickness $d_2$. In figure 4, we have plotted the on-resonance transmission and reflection coefficients $|t_{14}|^2_{\rm res}$ and $|r_{14}|^2_{\rm res}$ as a function of $d_2$, for different values of the losses (i.e. of $n_3''$). In these curves, we can find the results of figure 3 corresponding to $d_2 = 700$ nm (dotted line). We also see that for a fixed value of $n_3''$, $|t_{14}|^2_{\rm res}$ reaches a maximum for an optimum value of $d_2$, while $|r_{14}|^2_{\rm res}$ goes to zero. For example, when $n_3'' = 10^{-4}$ (curve (2)), $|t_{14}|^2_{\rm res}$ is maximum for $d_2 = 800$ nm and is then equal to 2000. This suggests the distinction between two regimes. When $d_2$ is much smaller than the optimum value, $|t_{14}|^2_{\rm res}$ increases exponentially with $d_2$. We will refer to this regime as 'low loss'. In the opposite situation, when $d_2$ is much larger than the optimum value, $|t_{14}|^2_{\rm res}$ decreases exponentially with $d_2$: this will be called the 'high-loss' regime. Note that the boundary between the two regimes depends on the value of $n_3''$: the optimum value of $d_2$ decreases when the losses increase, and so does the maximum value of $|t_{14}|^2_{\rm res}$.

We can again interpret these results with the Fabry–Perot analogy including losses inside the cavity. For a given coupling mirror, the build-up in the cavity will be reduced and the finesse will decrease when the losses increase. If the losses are fixed and the thickness of the gap $d_2$ is varied, a maximum for the electric field build-up will be reached when the transmission coefficient of the coupling mirror equals the losses per round trip inside the cavity: this is similar to an impedance matching condition. This explains qualitatively why there is a maximum in $|t_{14}|^2_{\rm res}$ as a function of $d_2$, and why the matching value of

$d_2$ decreases with the losses. We can also understand why $|r_{14}|^2_{\text{res}}$ goes to zero when the matching condition is fulfilled: in this situation, the light directly reflected on the coupling mirror destructively interferes with the light stored in the cavity and transmitted back through the coupling mirror.

### *2.5. Lorentzian approximation*

*2.5.1. Approximations.* In this section, we want to derive simplified expressions for the transmission and reflection coefficients $|t_{14}|^2$ and $|r_{14}|^2$ to show more explicitly their dependence on the gap thickness $d_2$ and in the losses via $n_3''$. In particular, we will obtain analytical expressions for the on-resonance values $|t_{14}|^2_{\text{res}}$ and $|r_{14}|^2_{\text{res}}$ and for the width $\Delta\lambda$ of the resonance peak. We will discuss their behaviour with $n_3''$ and $d_2$, and gain a quantitative insight into the results previously discussed with the Fabry–Perot analogy. This will also allow us to simply relate the two coefficients $|t_{14}|^2$ and $|r_{14}|^2$ with respect to each other.

In order to simplify the expressions, we assume that the 'low coupling' condition is fulfilled:

$$\exp(-2\kappa_2 d_2) \ll 1 \tag{22}$$

and that the losses in the waveguide remain small, which amounts to (see the appendix):

$$n_3'' \ll 1\,. \tag{23}$$

In our experimental situation ($d_2 = 700$ nm and $\lambda = 780$ nm), $\exp(-2\kappa_2 d_2) = 4\times10^{-4}$ and $n_3''$ will vary between $10^{-5}$ and a few times $10^{-4}$: both quantities are small and of the same order of magnitude. Therefore, we will expand the expressions of $|t_{14}|^2$ and $|r_{14}|^2$ at the lowest order in $n_3''$ and in $\exp(-2\kappa_2 d_2)$, neglecting the terms of order $n_3''\exp(-2\kappa_2 d_2)$.

We will then focus our interest on the behaviour of $|t_{14}|^2(\lambda)$ and $|r_{14}|^2(\lambda)$ around resonance, and approximate these functions by their lowest-order expansion in $\lambda$. We will end up with a Lorentzian dependence on $\lambda$ for $|t_{14}|^2$ and $|r_{14}|^2$ around resonance. Note that similar Lorentzian expressions could be obtained for $|t_{14}|^2(\theta_1)$ and $|r_{14}|^2(\theta_1)$.

*2.5.2. Calculation of $|t_{14}|^2(\lambda)$ and $|r_{14}|^2(\lambda)$.* In this section, we will expand $|t_{14}|^2$ and $|r_{14}|^2$ to lowest order in $n_3''$ and $\exp(-2\kappa_2 d_2)$, and then around the resonance in $\lambda$. Here we will give the main steps of the calculation for $|t_{14}|^2$, and refer to the appendix for more details. The expansion of $|r_{14}|^2$ is very similar and we will only give the final expression.

We start from expression (13) which we write in the form

$$|t_{14}|^2 = \frac{|t_{12}t_{23}t_{34}\exp(\mathrm{i}k_{z3}d_3)|^2\exp(-2\kappa_2 d_2)}{|F + G\exp(-2\kappa_2 d_2)|^2} \tag{24}$$

where $F$ and $G$ are given by (14) and (15). Note that $k_{z3}$, given by (3), is no longer a real number but has an imaginary part proportional to $n_3''$.

The full dependence on $\exp(-2\kappa_2 d_2)$ is explicit in expression (24). Because we neglect the terms of order $n_3''\exp(-2\kappa_2 d_2)$, we only have to consider the dependence on $n_3''$ in the term $F$. This dependence appears through the Fresnel coefficients $r_{3j}$ and the $z$ component of the wave vector in the waveguide $k_{z3}$. To first order in $n_3''$, we have (see the appendix):

$$F = 1 - (1 - an_3'')\exp(\mathrm{i}\Psi) \tag{25}$$

where $\Psi$ is the same as in (19), and $a$ is a numerical factor depending on the indices and the incidence angle (see the appendix, equation (A8)). We have seen in section 2.3 that the resonance condition corresponds, in the 'low-coupling' regime and in the absence of losses, to $F = 0$ and, in the case of the lowest-order mode, to $\Psi = 0$. In equation (25), we see

that the lowest-order approximation in $n_3''$ results in an attenuation of the electric field of $an_3''$ per round trip inside the waveguide, while the phase term in $F$ is not modified.

We now want to analyse the behaviour of $|t_{14}|^2$ as a function of the wavelength around the resonance. In expression (24), the dependence of $|t_{14}|^2$ on $\lambda$ is, around resonance, mainly due to the phase term $\Psi$. We will thus expand $\Psi$ around the resonance wavelength $\lambda_{\rm res}^0$ for the 'uncoupled' waveguide, for which $\Psi = 0$. We limit the expansion to the lowest order in $\lambda - \lambda_{\rm res}^0$:

$$\Psi \approx \left(\lambda - \lambda_{\rm res}^0\right) \left.\frac{\partial \Psi}{\partial \lambda}\right|_{\lambda_{\rm res}^0} \equiv \left(\lambda - \lambda_{\rm res}^0\right) \chi \ll 1 \,. \tag{26}$$

In our system, $\chi = 2.5$ mrad nm$^{-1}$ at 780 nm, so this approximation remains justified even several tens of nanometres away from resonance. We neglect the terms of order $\Psi \exp(-2\kappa_2 d_2)$ and $\Psi n_3''$. Note that $\chi$ not only includes the explicit dependence of $k_{z3}$ on $\lambda$, but also the variations of the phase shifts $\Phi_{32}$ and $\Phi_{34}$ through the dispersion of the indices of refraction. Taking into account all these simplifications we eventually obtain (see the appendix):

$$|t_{14}|^2 = |t_{14}|_{\rm res}^2 \frac{\Delta\lambda^2}{(\lambda - \lambda_{\rm res})^2 + \Delta\lambda^2} \tag{27}$$

with

$$\lambda_{\rm res} = \lambda_{\rm res}^0 + \frac{2\exp(-2\kappa_2 d_2)\sin 2\Phi_{32}\cos 2\Phi_{12}}{\chi} \tag{28}$$

$$\Delta\lambda = \frac{an_3'' + 2\exp(-2\kappa_2 d_2)\sin 2\Phi_{12}\sin 2\Phi_{32}}{|\chi|} \tag{29}$$

$$|t_{14}|_{\rm res}^2 = \frac{64\cos^2\Phi_{12}\cos^2\Phi_{34}\sin^2\Phi_{32}\exp(-2\kappa_2 d_2)}{\chi^2\left(an_3'' + 2\exp(-2\kappa_2 d_2)\sin 2\Phi_{12}\sin 2\Phi_{32}\right)^2} \,. \tag{30}$$

In expression (27), the quantities $\lambda_{\rm res}$, $\Delta\lambda$ and $|t_{14}|_{\rm res}^2$ vary slowly with $\lambda$ through $\exp(-2\kappa_2 d_2)$ and the dispersion of the refractive indices; however, the main dependence on $\lambda$ of $|t_{14}|^2$ around resonance appears explicitly in (27). Therefore we consider the quantities $\lambda_{\rm res}$, $\Delta\lambda$ and $|t_{14}|_{\rm res}^2$ constant and equal to their values in $\lambda = \lambda_{\rm res}^0$. Then, the transmission factor $|t_{14}|^2$ assumes a Lorentzian shape around resonance, which is characterized by three parameters: the position of the resonance $\lambda_{\rm res}$, the half-width at half maximum $\Delta\lambda$ and the on-resonance (maximum) value $|t_{14}|_{\rm res}^2$.

Starting from expression (16) and using the same approximations, we find for the reflection coefficient (see the appendix)

$$|r_{14}|^2 = 1 - \left(1 - |r_{14}|_{\rm res}^2\right) \frac{\Delta\lambda^2}{(\lambda - \lambda_{\rm res})^2 + \Delta\lambda^2} \tag{31}$$

with

$$|r_{14}|_{\rm res}^2 = \frac{\left(an_3'' - 2\sin 2\Phi_{12}\sin 2\Phi_{32}\exp(-2\kappa_2 d_2)\right)^2}{\left(an_3'' + 2\sin 2\Phi_{12}\sin 2\Phi_{32}\exp(-2\kappa_2 d_2)\right)^2} \,. \tag{32}$$

Thus, we see that the reflectivity curve $|r_{14}|^2(\lambda)$ is the complement of a Lorentzian around resonance, with the same width $\Delta\lambda$ as $|t_{14}|^2(\lambda)$.

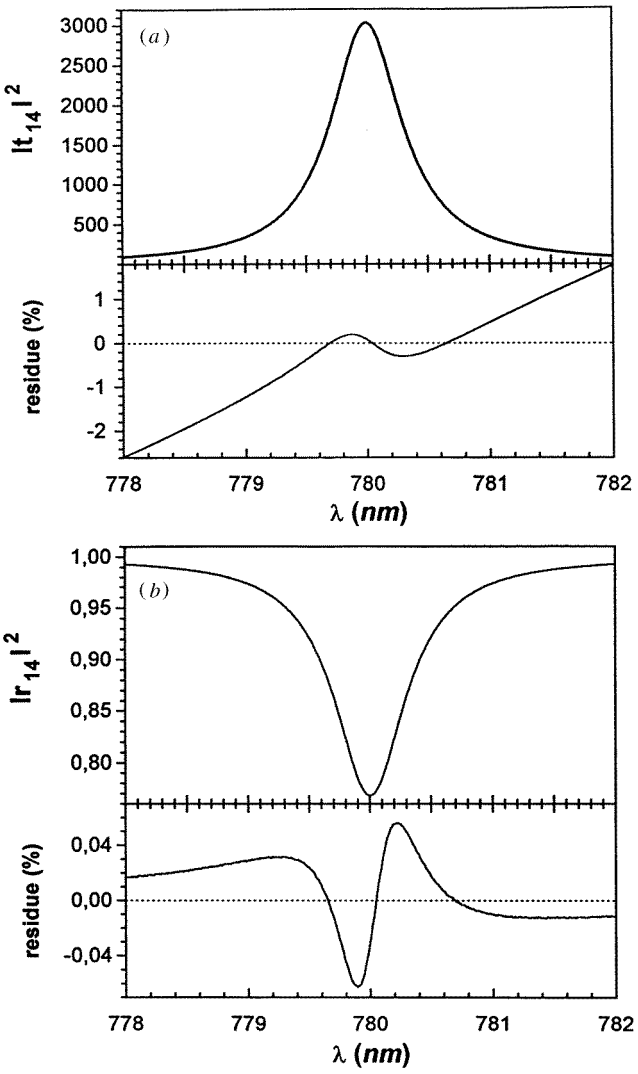


**Figure 5.** Comparison between the results of the exact calculation (equations (13) and (16)) and the Lorentzian approximation, (*a*) for the transmission factor $|t_{14}|^2$ ($\lambda$) and (*b*) for the reflection coefficient $|r_{14}|^2$ ($\lambda$). For these curves, $d_2 = 700$ nm and $n_3'' = 2 \times 10^{-5}$. The curves are not distinguishable on this scale; the relative differences (residues) are plotted below each curve.

*2.5.3. Discussion.* In order to quantify the validity of the Lorentzian approximation, we compare in figure 5 the transmission and reflection curves obtained with the exact Fresnel formulae (13) and (16) with the approximated expressions (27) and (31). On the scale of the figure, the curves are indistinguishable. We have also plotted the relative difference between the exact and approximated curves. These differences arise primarily from the wavelength dependence of the term $\exp(-2\kappa_2 d_2)$, which we have neglected in expressions (28)–(30) and (32).

We can now use the analytical expressions (28)–(30) and (32), obtained through the Lorentzian approximation, to discuss the dependence on $n_3''$ and $d_2$.

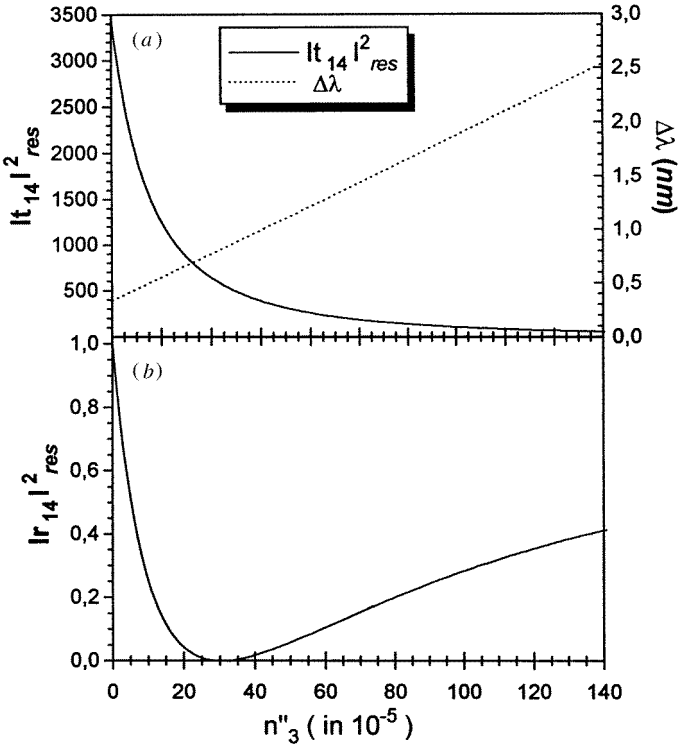


**Figure 6.** (*a*) On-resonance transmission $|t_{14}|^2_{\rm res}$ and resonance width $\Delta\lambda$ and (*b*) on-resonance reflection $|r_{14}|^2_{\rm res}$ as a function of $n_3''$. These curves are plotted using the results of the Lorentzian approximation, with the nominal values of the parameters of the structure (see figure 1).

Equation (28) shows that the resonance wavelength for the structure $\lambda_{\rm res}$ is equal to the resonance wavelength for the 'uncoupled' waveguide $\lambda^0_{\rm res}$, plus a term proportional to $\exp(-2\kappa_2 d_2)$. This term, reflecting the effect of the finite thickness of the gap $d_2$, was neglected in the qualitative discussion of section 2.3. In our system, this displacement of the resonance is about 0.1 nm. As expected, the resonance wavelength is independent of the losses, since $n_3''$ did not induce any additional phase shift in the lowest-order expansion of $\Psi$.

In the loss-free case $n_3'' = 0$, both the inverse of the resonance width $\Delta\lambda$ and the on-resonance transmission factor $|t_{14}|^2_{\rm res}$ are proportional to $\exp(+2\kappa_2 d_2)$. This behaviour was outlined in section 2.3 using the Fabry–Perot analogy. Figure 6 shows the variations of $|t_{14}|^2_{\rm res}$, $\Delta\lambda$ and $|r_{14}|^2_{\rm res}$ for increasing values of the losses, and a fixed gap thickness $d_2 = 700$ nm. The resonance width increases linearly with $n_3''$ while $|t_{14}|^2_{\rm res}$ decreases continuously to zero.

In the three expressions (29), (30) and (32), we clearly see the appearance of the two different regimes introduced in section 2.4: as long as $2\exp(-2\kappa_2 d_2)\sin 2\Phi_{12}\sin 2\Phi_{32} \gg an_3''$, $|t_{14}|^2_{\rm res}$ exponentially increases with $d_2$; this is the 'low-loss' regime. When $2\exp(-2\kappa_2 d_2)\sin 2\Phi_{12}\sin 2\Phi_{32} \ll an_3''$ (i.e. in the 'high-loss' regime), $|t_{14}|^2_{\rm res}$ exponentially decreases when $d_2$ increases. Thus, with the Lorentzian approximation, we have obtained the analytical condition which determines the boundary between the two regimes:

$$an_3'' = 2\exp(-2\kappa_2 d_2)\sin 2\Phi_{12}\sin 2\Phi_{32}\,. \tag{33}$$

This corresponds to the matching condition in a Fabry–Perot, where $an_3''$ is the loss per round trip, and $2\exp(-2\kappa_2 d_2)\sin 2\Phi_{12}\sin 2\Phi_{32}$ represents the coupling into the cavity. In expression (32), condition (33) yields $|r_{14}|^2_{\mathrm{res}} = 0$.

*2.5.4. Relationship between $|t_{14}|^2_{\mathrm{res}}$ and $|r_{14}|^2(\lambda)$.* It can be seen from expressions (29), (30) and (32) that the quantities characterizing the transmission and reflection resonance curves involve the same parameters: $\exp(-2\kappa_2 d_2)$, $n_3''$ and $\chi$. Therefore it is possible to express the on-resonance transmission factor $|t_{14}|^2_{\mathrm{res}}$ in terms of the characteristics of the reflectivity curve:

$$|t_{14}|^2_{\mathrm{res}} = \beta\frac{\left(1 \pm \sqrt{|r_{14}|^2_{\mathrm{res}}}\right)}{\Delta\lambda}. \tag{34}$$

The factor $\beta$ is given by

$$\beta = 4\cos^2\Phi_{34}\frac{\tan\Phi_{32}}{\tan\Phi_{12}}\frac{1}{|\chi|}. \tag{35}$$

The plus and minus signs in (34) correspond, respectively, to the low-loss and high-loss regimes. When the matching condition (33) is fulfilled, $|r_{14}|^2_{\mathrm{res}} = 0$. Note that, in the low-loss regime, if $|r_{14}|^2_{\mathrm{res}}$ is close to 1, $|t_{14}|^2_{\mathrm{res}}$ is simply inversely proportional to $\Delta\lambda$.

The quantities $|r_{14}|^2_{\mathrm{res}}$ and $\Delta\lambda$ can be obtained by experimentally recording the reflectivity of the structure as a function of the wavelength. The factor $\beta$ is a slowly varying function of the indices and thicknesses of the dielectric layers, and does not depend on $n_3''$. All the 'resonant' character of $|t_{14}|^2_{\mathrm{res}}$ is contained in $\Delta\lambda$ and $|r_{14}|^2_{\mathrm{res}}$, both quantities which can be easily measured experimentally. Therefore, equation (34) can be conveniently used to estimate $|t_{14}|^2_{\mathrm{res}}$, even when the indices and thicknesses of the layers are not known very precisely.

## 3. Experimental section

In this part of the paper, we describe in detail our method for evaluating the enhancement of the evanescent wave, based on the analysis of the reflected beam intensity. We first describe our experimental procedure for recording the reflectivity curve, together with an example of experimental data. The next section is devoted to the analysis of the experimental data, eventually yielding a numerical value for $|t_{14}|^2_{\mathrm{res}}$. The accuracy of this result is discussed. Finally, we describe the observed evolution of the resonance with time, and propose an interpretation for this behaviour.

### *3.1. Experimental procedure and results*

The evaluation of the performance of our waveguide is based on the measurement of the reflection coefficient $|r_{14}|^2$ as a function of the wavelength $\lambda$. This measurement is performed using the experimental set-up illustrated in figure 7. A Ti:sapphire laser beam with a typical power of 100 mW enters the prism and reflects from the layered structure. The intensity of the reflected beam is recorded with a photodetector as the wavelength of the laser is scanned across resonance.

Our aim is to evaluate the enhancement of the evanescent wave in the conditions of the atomic mirror experiments; this is why the measurement takes place inside the UHV chamber used for these experiments. To perform this measurement, we need to control the

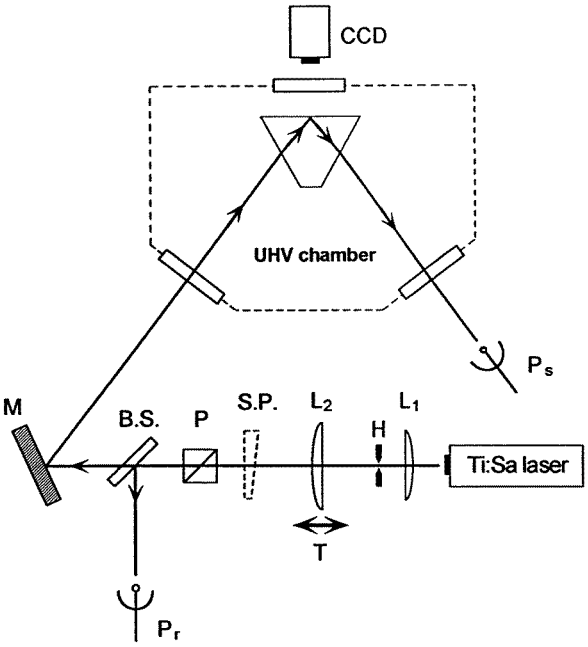


**Figure 7.** Experimental scheme for the *in situ* recording of the reflectivity curves. The prism is inside a UHV chamber. The beam from a Ti:Sa laser experiences total internal reflection inside the prism and its intensity is measured with the photodetector $P_s$; a fraction of the incident light is sent on the photodetector $P_r$. The laser beam passes through a telescope ($\gamma = 3$) with a spatial filter (H); after the telescope, the beam waist is 2.28 mm. The incident laser power was 100 mW. The collimation of the beam is optimized by adjusting the position of the output lens $L_2$, using a shear-plate interferometer S.P. temporarily placed in the front focal plane of $L_2$. The incident light polarization (TE) and angle of incidence are adjusted by monitoring the light scattered in the waveguide with a CCD camera.

parameters that characterize the incident laser beam: the internal angle of incidence $\theta_1$, the angular divergence of the laser beam, its polarization and wavelength.

The angle of incidence is adjusted using the mirror (M) mounted on an orientation stage. Its value is measured using the reflection of the incident beam on the input face of the prism, with an accuracy of $\pm 0.2$ mrad.

In the theoretical section, we considered the case of an incident plane wave. However, since the angular width of the resonance is very small (HWHM: $\Delta\theta_1 = 0.21$ mrad), the divergence of the laser beam used for the measurement is not negligible. As a consequence, it is necessary to deconvolve the measured reflectivity curve, which requires good control of the divergence angle. For this purpose the beam provided by the laser passes through a telescope whose output lens ($L_2$) position can be adjusted. A spatial filter (H) is placed at the focal point inside the telescope. The minimum for the output beam divergence is obtained when the spatial filter is in the back focal plane of lens $L_2$, which corresponds to an output beam waist in the front focal plane of $L_2$. To adjust the proper position for the lens $L_2$, we use a shear-plate interferometer (S.P.) [19], placed in the front focal plane of the lens. The resulting divergence has been measured by looking at the beam profile with a CCD camera, at different positions on the propagation axis. The fit of the data by a Gaussian-beam law yields a waist size $w_0 = 2.28$ mm and a divergence of 0.064 mrad (HWHM), outside the prism. Due to the high refractive index of the prism ($n_1 = 1.893$), the

divergence angle inside the prism is 0.034 mrad, which must be compared to the angular width of the resonance $\Delta\theta_1 \simeq 0.21$ mrad. Therefore the width of the angular spectrum of the incident beam is approximately six times smaller than the angular width of the resonance.

The incident light polarization is determined by a polarizing cube (P) mounted on a rotation stage. The extinction ratio of the cube is $10^{-4}$ in transmission.

The spectrum of the laser beam is monitored with a Fabry–Perot analyser (free spectral range 750 MHz). Thus, we can verify that the laser remains single mode when the wavelength is varied. The emission wavelength of the laser is measured with a wavemeter, with an accuracy of $\pm 0.01$ nm.

The procedure for the measurement of the reflectivity curve is as follows. First, the angle of incidence is adjusted to obtain the resonance for $\lambda = 780$ nm. The proper orientation for the polarization is then adjusted. These operations are achieved by looking at the surface of the prism from above with a CCD camera; when the electric field builds up inside the waveguide layer due to the resonance, the scattered light strongly increases and the impact of the beam on the prism surface appears as a bright spot.

It is essential to get rid of the intensity fluctuations of the incident laser beam. A beamsplitter (B.S.), placed after the polarizing cube, sends a portion of the incident light on a first photodetector ($P_r$) to provide a reference for the incident light intensity. After reflection inside the prism, the laser beam is collected on a second detector ($P_s$). The outputs of both detectors are fed to a LeCroy numerical oscilloscope which calculates the ratio $P_s/P_r$. An averaging over 100 sweeps reduces the small amplitude noise left on the signal after division. The final reproducibility of the signal is well below one per cent.

When recording reflectivity curves, we usually observe a small asymmetry (a few per cent) between the baselines on each side of the resonance. One possible cause for this behaviour is a slow drift of the alignment of the Ti:Sa laser cavity, due, for example, to thermal phenomena in the crystal or displacement of the argon laser pump beam. To minimize that problem, we let the laser warm up for some time and stabilize. The remaining asymmetry, when present, is corrected assuming a linear variation with the wavelength. The resulting reflectivity curve is normalized so that its off-resonance value is equal to 1.

In figure 8, we present a typical example of an experimental reflectivity curve; the full circles correspond to TE polarization, and the curve with open circles was obtained with TM polarization; as expected, it exhibits no resonant behaviour. The experimental curve in TE polarization is the result of the convolution of a Lorentzian (i.e. the plane-wave response of the prism given by equation (31)) by a Gaussian (i.e. the angular spectrum of the incident beam, which has been measured). We therefore fit the experimental data with a Voigt profile. To convert the angular profile of the laser beam into an equivalent spectral profile, we need to know the quantity:

$$s = \frac{\partial\theta_{1\mathrm{res}}}{\partial\lambda} \,. \tag{36}$$

We obtain this quantity experimentally, by recording the resonance angle of incidence $\theta_{1\mathrm{res}}$ at various wavelengths (see figure 9). The fitted Voigt profile is shown in figure 8 (full curve); it is characterized by the position $\widetilde{\lambda}_{\mathrm{res}}$ and the value $|\widetilde{r_{14}}|^2_{\mathrm{res}}$ of the minimum, and by the half-width at half-maximum $\widetilde{\Delta\lambda}$. These quantities could be directly measured on the experimental curve. After the deconvolution, we obtain the corresponding characteristics of the Lorentzian plane-wave response $\lambda_{\mathrm{res}}$, $\Delta\lambda$ and $|r_{14}|^2_{\mathrm{res}}$.

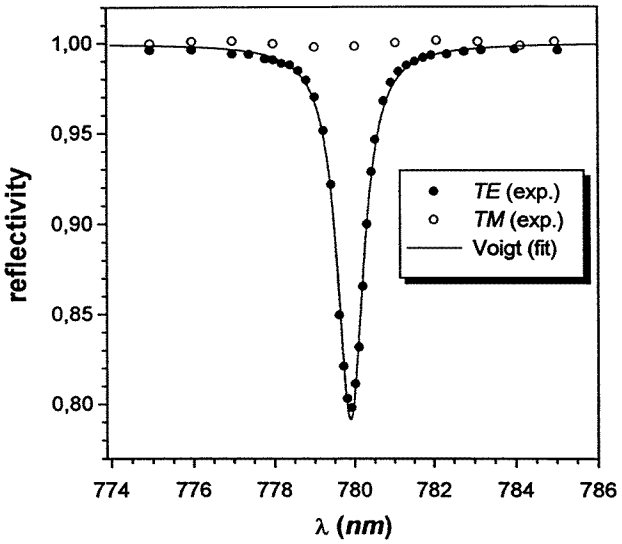


**Figure 8.** Typical experimental reflectivity curve for the structure shown in figure 1. The open circles correspond to TM polarization where no resonance occurs. The full circles correspond to TE polarization. The statistical uncertainty of the data points is about the size of the circles. The resonance curve is fitted by a Voigt profile including the measured angular divergence of the incident laser beam (0.069 mrad HWHM). The fitted parameters (before deconvolution) are: $\widetilde{\lambda}_{\rm res} = 780.00$ nm, $\widetilde{\Delta\lambda} = 0.751$ nm and $|\widetilde{r_{14}}|^2_{\rm res} = 0.777$. The corresponding characteristics of the Lorentzian profile are: $\lambda_{\rm res} = 780.00$ nm, $\Delta\lambda = 0.73$ nm and $|r_{14}|^2_{\rm res} = 0.772$.

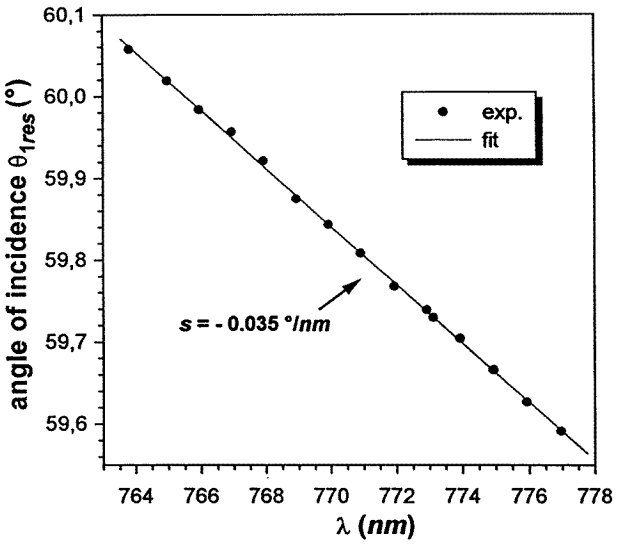


**Figure 9.** Measurement of the variation of the resonance angular position $\theta_{1\,\rm res}$ with the wavelength $\lambda$. The slope $s$ of this curve is used for the deconvolution of the experimental data. Our set-up did not permit the measurement of the angle of incidence around $\lambda_{\rm res} = 780$ nm. The linearity of the curve over the 15 nm range shown allows us to extrapolate to the value at $\lambda_{\rm res} = 780$ nm.

### *3.2. Analysis of the measurements*

We now present a first method for analysing the experimental data, with the goal of obtaining an accurate value for the enhancement factor. This method can be summarized as follows.

We compute the transmission and reflection coefficients $|t_{14}|^2(\lambda)$ and $|r_{14}|^2(\lambda)$, using the exact expressions in the case of an incident plane wave (13) and (16). The parameters that characterize the structure (e.g. the thicknesses and indices of the dielectric layers) are adjusted to fit the experimental data. The enhancement factor can then be calculated, using the fitted values of these parameters.

This approach is motivated by two observations. First, the nominal values (i.e. provided by the manufacturer) of the thicknesses and indices of the layers are not known to better than 1%. In addition, the value of $n_3''$ is not available, and somewhat difficult to estimate *a priori*. These uncertainties on the parameters of the structure would yield, for our highly resonant structure, an unacceptably large uncertainty on the calculated transmission factor. Second, we have observed strong modifications of the characteristics of the resonance with time, which we attribute to variations of the structure parameters (in particular, the losses). Thus, the parameters of the model have to be continuously readjusted to account for the observed behaviour.

In our model, the structure is *a priori* described by nine parameters, characterizing the prism ($n_1$, $\partial n_1/\partial\lambda$), the gap ($d_2$, $n_2$, $\partial n_2/\partial\lambda$) and the waveguide ($d_3$, $n_3'$, $\partial n_3/\partial\lambda$, $n_3''$). The parameters $\partial n_j/\partial\lambda$ take into account the dispersion of the indices of refraction:

$$n_j\,(\lambda \text{ in nm}) = n_j\,(\lambda = 780 \text{ nm}) - \frac{\partial n_j}{\partial\lambda}\,(\lambda - 780) \tag{37}$$

assuming a linear dependence for the limited range of wavelength explored. The measurement provides four quantities: $\widetilde{\lambda}_{\text{res}}$, $s$, $\widetilde{\Delta\lambda}$ and $|\widetilde{r_{14}}|^2_{\text{res}}$. Therefore, we need to narrow our choice of nine possible parameters to four that will be fitted.

Unlike the thin layers, whose parameters (e.g. the indices) are not known exactly, the refractive index $n_1$ of the prism has been precisely measured, yielding

$$n_1\,(\lambda \text{ in nm}) = 1.8934 - 7.39 \times 10^{-5} \times (\lambda - 780)\,. \tag{38}$$

Although the value of the dispersion for the gap is not known precisely, its influence can be neglected. Thus, we now have to choose between six parameters to adjust: $d_2$, $d_3$, $n_2$, $n_3'$, $\partial n_3/\partial\lambda$ and $n_3''$. It is clear from the discussion above that $n_3''$ has to be adjusted. We select among the remaining parameters those which have the strongest influence on the measured quantities; for instance, since the value of $\partial n_1/\partial\lambda$ is fixed, it is the parameter $\partial n_3/\partial\lambda$ which has the main influence on the quantity $s = \partial\theta_{1\text{res}}/\partial\lambda$. Therefore, we will retain $\partial n_3/\partial\lambda$ as a fit parameter. Finally, the indices $n_2$ and $n_3'$ have somewhat more influence than $d_2$ and $d_3$ on the measured quantities. Therefore our fitting parameters are: $n_2$, $n_3'$, $\partial n_3/\partial\lambda$ and $n_3''$.

The fitting procedure operates as follows: the program starts from a set of layer parameters, for instance the set of nominal values. It computes the reflectivity curve for an incident plane wave, and the characteristic quantities $\theta_{1\text{res}}$, $\Delta\lambda$ and $|r_{14}|^2_{\text{res}}$ and $s$. These are compared to the experimental values obtained after deconvolution of the experimental curve. The layer parameters $n_2$, $n_3'$, $\partial n_3/\partial\lambda$ and $n_3''$ are then modified according to a simple Newton-type algorithm; the whole process is iterated until the experimental quantities are fitted.

We have applied this procedure to the experimental data presented in figures 8 and 9. The set of fitted structure parameters obtained is

$$\begin{aligned} &n_3'\,(\lambda = 780 \text{ nm}) = 2.386 \\ &\frac{\partial n_3}{\partial\lambda} = -3.39 \times 10^{-4} \\ &n_3'' = 2.46 \times 10^{-5} \\ &n_2\,(\lambda = 780 \text{ nm}) = 1.509\,. \end{aligned} \tag{39}$$

Note that the values obtained for the indices $n_3'$ and $n_2$ of the layers agree with the nominal values (see figure 1) within the uncertainty range provided by the manufacturer (1%). Using these fitted parameters in equation (13), we calculate the value of the transmission factor (for an incident plane wave):

$$|t_{14}|^2_{\mathrm{res}} = 2360\,. \tag{40}$$

We now address the question of the uncertainty on this transmission factor. The fitting procedure described above uses fixed values of the structure parameters that are not fitted (i.e. $d_2$, $d_3$ and $\partial n_2/\partial\lambda$), and of the experimental quantities (i.e. $\theta_{1\mathrm{res}}$, $\lambda_{\mathrm{res}}$, $\Delta\lambda$, $|r_{14}|^2_{\mathrm{res}}$ and $s$). All these quantities are known with limited precision, which results in a global uncertainty on the final calculated value of $|t_{14}|^2_{\mathrm{res}}$. Using the same fitting procedure, we numerically estimate the partial derivatives of $|t_{14}|^2_{\mathrm{res}}$ with respect to each of these quantities. This allows us to obtain the uncertainty on $|t_{14}|^2_{\mathrm{res}}$, knowing the uncertainties on the relevant nominal and experimental parameters. The main contributions to this final uncertainty are due to the nominal uncertainties on $d_2$ and $d_3$ (1%), and to the experimental uncertainties on the resonance width ($\simeq 0.01$ nm) and on the on-resonance reflection coefficient ($\simeq 0.01$).

We finally obtain

$$|t_{14}|^2_{\mathrm{res}} = 2360 \pm 150\,. \tag{41}$$

We can define an enhancement factor as the ratio of the squared amplitude of the electric field in the evanescent wave above the prism with and without the dielectric layers, for the same intensity and polarization of the incident laser beam [14]. This quantity is simply the ratio of the transmission factors with and without the dielectric layers. Since the transmission factor for a bare prism is 1.43 in our conditions (TE polarization, $\theta_1 \simeq 59^\circ$), the enhancement factor is equal to 1650. This can be considered as the gain in available laser power achieved with the resonant waveguide structure.

As discussed in section 2.5.4, one could more simply estimate the on-resonance transmission factor using equation (34). In this equation, the factor $\beta$ can be calculated with expression (35), using the nominal values for the parameters of the layers and the measured values of $\lambda_{\mathrm{res}}$ and $\theta_{1\mathrm{res}}$. The quantities $\Delta\lambda$ and $|r_{14}|^2_{\mathrm{res}}$ are obtained from the deconvolution of the experimental data, using the slope $s$ measured in figure 9. Applying this method to the measurement of figure 8, we find $|t_{14}|^2_{\mathrm{res}} = 2318$. We see that this phenomenological analysis of the experimental reflectivity curve is very convenient to easily obtain an estimation of the transmission factor. Unlike the detailed analysis described before, however, this approach provides no information on the values of the various parameters of the structure. Indeed one must assume their nominal values to estimate $|t_{14}|^2_{\mathrm{res}}$.

Finally, note that the value given in (41) corresponds to the plane-wave response of the structure, and hence to the maximum transmission attainable with this system. To estimate the effective transmission factor $|\widetilde{t_{14}}|^2_{\mathrm{res}}$ obtained with an incident laser beam of finite waist size, one needs to make the convolution between the plane-wave response of the prism and the angular spectrum of the laser beam. For instance, with the same beam as used for the measurement of figure 8, we obtain $|\widetilde{t_{14}}|^2_{\mathrm{res}} = 2250$.

### *3.3. Evolution of the resonance*

The high finesse of our structure makes it very sensitive to small variations of its parameters (e.g. the losses or the thicknesses of the layers). We have observed, in the course of a series of experiments on the reflection of rubidium atoms on the enhanced evanescent wave [11], a pronounced evolution of the performance of the waveguide structure. This evolution was

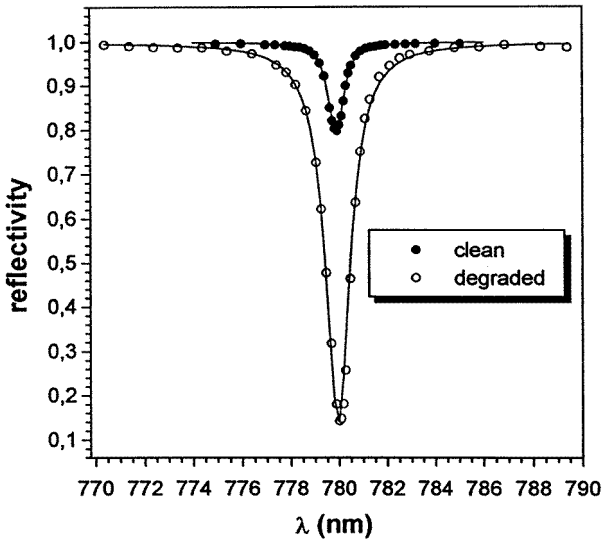


**Figure 10.** Illustration of the evolution of the resonance with time. The full symbols correspond to a recently cleaned prism, and the open symbols to the same structure after 2 months of experiments with rubidium atoms.

correlated with the operation of the decelerated atomic beam and hence to the presence of Rb atoms inside the vacuum chamber above the prism. The general features of the evolution were an increase of the width of the reflectivity curve and a decrease of the on-resonance reflection coefficient. This is illustrated in figure 10, where we show two experimental resonance curves corresponding to a recently cleaned prism and a 'degraded' prism, respectively. The time between the two measurements corresponds to 2 months of experiments with the atoms. We have found that this phenomenon can be reversed by cleaning the surface of the prism. This was achieved using two different techniques: a 'mechanical' cleaning, where the prism was removed from the vacuum chamber and carefully wiped with an optical tissue and solvents, and a 'thermal' cleaning where the prism was heated between 50 and 100 °C for two days, inside the vacuum chamber, using heating lamps intended for the baking of the chamber. In both cases, the effect of the cleaning was to restore the initial reflectivity curve. These observations support the interpretation that the evolution of the resonance is due to the pollution of the waveguide surface.

It seems reasonable to represent the effect of the pollution of the waveguide by an increase of the losses, and hence of $n_3''$. To check this model, we have plotted in figure 11 the on-resonance reflection coefficient $|r_{14}|^2_{\mathrm{res}}$ as a function of the width $\Delta\lambda$, as expected from our model when only $n_3''$ is increased (full curve). We also plot the results of the *in situ* measurements performed on the prism, extending over a period of 9 months (full circles). Note that, during this period, the prism was removed from the vacuum chamber and cleaned twice using the methods described above. Considering the fact that the theoretical curve includes no fitting parameters, the agreement is reasonably good. The most important difference is that the measured reflectivity never reaches zero. A possible explanation for this discrepancy may be the inability of our model to describe the losses by scattering with an imaginary part of the refractive index of the waveguide. In our model, the scattered light disappears like the absorbed light, while in the real situation part of it might be scattered back in the reflected beam and result in an offset of the reflectivity curve.

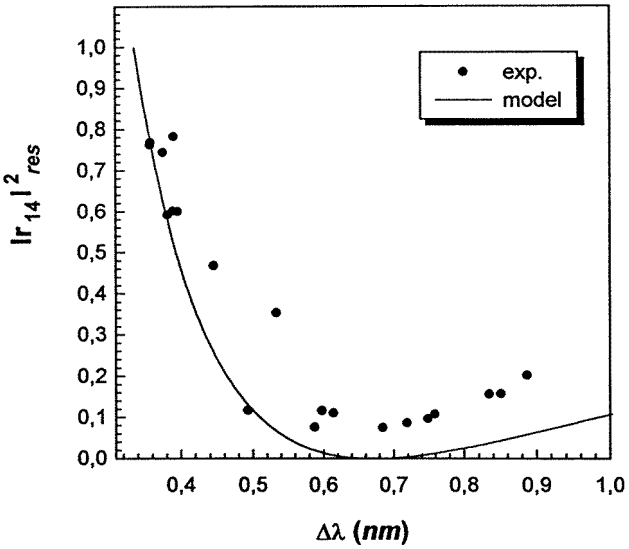


**Figure 11.** Measured values of $|r_{14}|^2_{\text{res}}$ versus $\Delta\lambda$ at various points during nine months of the prism's history. The measured on-resonance reflection coefficient $|r_{14}|^2_{\text{res}}$ is plotted as a function of the measured width of the resonance $\Delta\lambda$ (full symbols). The full curve corresponds to the theoretical evolution when only $n_3''$ is varied.

## 4. Conclusion

In this paper, we have both theoretically and experimentally investigated the properties of a structure providing large enhancements of an evanescent wave. With this new structure, we have achieved a 10-fold improvement of the enhancement compared to our first prototype [14]. We obtain a value of the on-resonance transmission factor of $|t_{14}|^2_{\text{res}} = 2360 \pm 150$, corresponding to an enhancement factor of 1650 for the evanescent wave intensity, compared to a bare prism. To understand the behaviour of such high-finesse systems, we had to take into account the losses, which led to the appearance of different regimes for the enhancement depending on the relative values of the losses and the coupling. In the regime of 'low coupling', we derived some simple approximate expressions for the quantities characteristic of the resonance, allowing for a detailed understanding of the role played by the various parameters. In the experimental part, we described our method for evaluating the enhancement factor, based on the analysis of the intensity of the reflected light. This technique of characterization has the advantage of allowing for a fairly easy *in situ* monitoring of the enhancement of the evanescent wave.

It is theoretically possible to obtain even higher enhancement values, by further increasing the gap thickness: for our clean prism, the fitted value of $n_3''$ ($2.5 \times 10^{-5}$, see equation (39)) suggests a maximum transmission factor $|t_{14}|^2_{\text{res}}$ of about 10 000 (see figure 4). However, several factors will eventually limit the enhancement: the divergence of the incident laser beam will have to be reduced, the sensitivity of the system to mechanical vibrations and to the pollution of the surface will increase, and the material of the waveguide layer might be altered by the heating due to residual absorption.

Here, we have studied the global transmission and reflection coefficients averaged over the surface of the laser beam. One might also want to study the spatial intensity distribution.

We have, for instance, observed structures in the reflected beam, appearing around resonance. These structures, obtained with a well collimated incident laser beam, differ in orientation and shape from the well known 'm-line' observed when the divergence of the beam is larger than the resonance width [20]. They might be due, for example, to small non-uniformities in the thicknesses of the layers.

**Acknowledgments**

This work was partly supported by DRET, THOMSON-CSF-LCR, EEC and the Ultimatech program of the CNRS. We also thank the company SAGEM for providing us with the IAD coatings.

**Appendix. Transmission and reflection coefficients in the Lorentzian approximation**

This appendix is devoted to the detailed derivation of $|t_{14}|^2(\lambda)$ and $|r_{14}|^2(\lambda)$ in the regime of 'low coupling', where $\exp(-2\kappa_2 d_2) \ll 1$, and for small losses, $n_3'' \ll 1$. As a consequence, we will expand the expressions at the lowest order in $n_3''$ and $\exp(-2\kappa_2 d_2)$.

Taking into account the losses in the waveguide has two consequences. Firstly, the $z$ component of the wave vector in the waveguide, $k_{z3}$, is now a complex quantity, given by (see equation (3))

$$(k_{z3})^2 = \left(n_3 \frac{\omega}{c}\right)^2 - (k_x)^2 \tag{A1}$$

where $k_x = n_1 \frac{\omega}{c} \sin\theta_1$ is real, as discussed in section 2.2, and $n_3$ is given in (21). The real part of $k_{z3}$ describes the phase evolution when the plane wave propagates inside the waveguide, while the imaginary part is responsible for the attenuation during the propagation. Expanding the real and imaginary parts of $k_{z3}$ in $n_3''$ and retaining only the lowest-order term, one obtains

$$\mathrm{Re}\,[k_{z3}] \approx \frac{\omega}{c}\sqrt{n_3'^2 - (n_1 \sin\theta_1)^2} \tag{A2}$$

and

$$\mathrm{Im}\,[k_{z3}] \approx \frac{\omega}{c}\sqrt{\frac{n_3'^2}{n_3'^2 - (n_1 \sin\theta_1)^2}}\, n_3'' . \tag{A3}$$

We also introduce the notation

$$\alpha = \frac{2\,\mathrm{Im}\,[k_{z3}]\, d_3}{n_3''} . \tag{A4}$$

With our parameters, the term $\alpha$ is of the order of 1. Equation (A2) shows that by neglecting the terms in $n_3''^2$, we have neglected the contribution of the losses to the phase shift during the propagation. On the other hand, we find that the attenuation of the wave during the propagation in the waveguide is proportional to $n_3''$.

The second effect of $n_3''$ is to modify the modulus and phase of the Fresnel coefficients for the reflection at the waveguide–gap and waveguide–vacuum interfaces [16]. Expanding the expressions of the Fresnel coefficients $r_{3j}$ in $n_3''$, one finds that the modulus $|r_{3j}|$ is modified by a first-order term in $n_3''$, while the modification of the phase $2\Phi_{3j}$ is only a second-order term in $n_3''$. Therefore, we see as before that, at the lowest-order in $n_3''$, we

take into account only the attenuation of the wave at reflection due to the losses, and not the phase modification. The calculation yields for the modulus of the Fresnel coefficients:

$$\left|r_{3j}\right| \approx 1 - \alpha_j n_3'' \approx \exp\left(-\alpha_j n_3''\right) \tag{A5}$$

where

$$\alpha_j = \frac{2\sqrt{(n_1 \sin\theta_1)^2 - n_j^2}}{((c/\omega)\mathrm{Re}\,[k_{z3}])^2 + (n_1 \sin\theta_1)^2 - n_j^2}\,. \tag{A6}$$

The factors $\alpha_j$ are typically of the order of 1 in our case. Thus, we now can write the term $r_{34}r_{32}\exp(2\mathrm{i}k_{z3}d_3)$, which describes the modification of the plane wave amplitude after one round trip inside the waveguide, as

$$r_{34}r_{32}\exp(2\mathrm{i}k_{z3}d_3) \approx \exp\left(-an_3''\right)\exp(\mathrm{i}\Psi) \tag{A7}$$

where

$$a = \alpha + \alpha_2 + \alpha_4\,. \tag{A8}$$

*Calculation of* $|t_{14}|^2$. We start from expression (13):

$$|t_{14}|^2 = \frac{|t_{12}t_{23}t_{34}\exp(\mathrm{i}k_{z3}d_3)|^2\exp(-2\kappa_2 d_2)}{|F + G\exp(-2\kappa_2 d_2)|^2} = \frac{N}{D} \tag{A9}$$

with

$$F = 1 - r_{34}r_{32}\exp(2\mathrm{i}k_{z3}d_3)$$
$$G = r_{12}r_{23} - r_{34}r_{21}\exp(2\mathrm{i}k_{z3}d_3)\,.$$

We can also write $G$ in the form

$$\begin{aligned} G &= r_{12}r_{23} - \frac{r_{21}}{r_{32}}r_{34}r_{32}\exp(2\mathrm{i}k_{z3}d_3) \\ &= r_{12}r_{23} - \frac{r_{21}}{r_{32}}(1 - F)\,. \end{aligned}$$

Thus, using the equality $r_{ji} = -r_{ij}$, we write for the denominator $D$ of expression (A9):

$$D = \left|\left(1 - \frac{r_{12}}{r_{32}}\exp(-2\kappa_2 d_2)\right)F + r_{12}\left(\frac{1}{r_{32}} - r_{32}\right)\exp(-2\kappa_2 d_2)\right|^2\,. \tag{A10}$$

Using the result of equation (A7), we write $F$ in the form

$$F \approx 1 - \exp\left(-an_3''\right)\exp(\mathrm{i}\Psi)\,. \tag{A11}$$

Since our aim is to obtain approximated expressions around resonance, we expand the phase shift per round trip $\Psi$ around the resonance wavelength $\lambda_{\mathrm{res}}^0$ of the 'uncoupled waveguide', at the lowest order:

$$\Psi(\lambda) \approx \chi\left(\lambda - \lambda_{\mathrm{res}}^0\right) \ll 1 \tag{A12}$$

where we have introduced the notation $\chi = (\partial\Psi/\partial\lambda)|_{\lambda_{\mathrm{res}}^0}$ and used the definition of the resonance wavelength $\Psi\left(\lambda_{\mathrm{res}}^0\right) = 0$. In the following we will neglect the cross-products of the form $\Psi n_3''$ and $\Psi\exp(-2\kappa_2 d_2)$. Equation (A11) then becomes

$$F \approx an_3'' - \mathrm{i}\Psi\,.$$

If we now turn back to expression (A10), we see that the first term of the sum simply becomes

$$\left(1 - \frac{r_{12}}{r_{32}}\exp(-2\kappa_2 d_2)\right)F \approx an_3'' - \mathrm{i}\Psi$$

and the second term is

$$r_{12}\left(\frac{1}{r_{32}}-r_{32}\right)\exp\left(-2\kappa_2 d_2\right)\approx 2\mathrm{i}r_{12}\sin 2\Phi_{32}\exp\left(-2\kappa_2 d_2\right).$$

Then, separating the real and imaginary parts, we finally obtain for the denominator $D$:

$$|D|^2\approx\chi^2\left[\lambda-\left(\lambda_{\mathrm{res}}^0+\frac{2\exp\left(-2\kappa_2 d_2\right)\sin 2\Phi_{32}\cos 2\Phi_{12}}{\chi}\right)\right]^2 + \left(\frac{an_3''+2\exp\left(-2\kappa_2 d_2\right)\sin 2\Phi_{12}\sin 2\Phi_{32}}{\chi}\right)^2. \tag{A13}$$

We now turn to the derivation of the numerator $N$ of $t_{14}$, as given by expression (A9):

$$N=\left|t_{12}t_{23}t_{34}\exp\left(\mathrm{i}k_{z3}d_3\right)\right|^2\exp\left(-2\kappa_2 d_2\right). \tag{A14}$$

We use the relationship between the amplitude Fresnel coefficients for transmission and reflection, that is, the continuity of the electric field at the interface:

$$t_{ij}=1+r_{ij}. \tag{A15}$$

Therefore, using the notation introduced in equation (9), one has

$$\left|t_{ij}\right|^2=\left(1+\left|r_{ij}\right|\cos 2\Phi_{ij}\right)^2+\left|r_{ij}\right|^2\sin^2 2\Phi_{ij}. \tag{A16}$$

According to (A5), the terms $|r_{32}|$ and $|r_{34}|$ both include a term proportional to $n_3''$. However, since the quantity $\exp\left(-2\kappa_2 d_2\right)$ is a factor in the expression of $N$, we can neglect the cross-products in $n_3''\exp\left(-2\kappa_2 d_2\right)$. Similarly, we neglect in $|\exp\left(\mathrm{i}k_{z3}d_3\right)|^2$ the terms in $n_3''$ and we obtain

$$N\approx 8\left(1+\cos 2\Phi_{21}\right)\left(1-\cos 2\Phi_{32}\right)\left(1+\cos 2\Phi_{34}\right)\exp\left(-2\kappa_2 d_2\right) = 64\cos^2\Phi_{12}\sin^2\Phi_{32}\cos^2\Phi_{34}\exp\left(-2\kappa_2 d_2\right). \tag{A17}$$

We have obtained an expression for $|t_{14}|^2(\lambda)$; in expressions (A13) and (A17), the main term describing the wavelength dependence of $|t_{14}|^2$ is the term $\lambda$ in $D$. All the other terms contribute little to the wavelength dependence of $|t_{14}|^2$ and can therefore be taken as constants, and replaced in (A13) and (A17) by their values in $\lambda=\lambda_{\mathrm{res}}^0$. Then, $|t_{14}|^2(\lambda)$ is maximum when $|D|^2(\lambda)$ is minimum, which corresponds to:

$$\lambda=\lambda_{\mathrm{res}}^0+\frac{2\exp\left(-2\kappa_2 d_2\right)\sin 2\Phi_{32}\cos 2\Phi_{12}}{\chi}=\lambda_{\mathrm{res}}. \tag{A18}$$

Thus, we finally obtain for the transmission factor $|t_{14}|^2(\lambda)$ a Lorentzian expression around resonance:

$$|t_{14}|^2(\lambda)\approx|t_{14}|_{\mathrm{res}}^2\frac{\Delta\lambda^2}{\left(\lambda-\lambda_{\mathrm{res}}\right)^2+\Delta\lambda^2} \tag{A19}$$

of width

$$\Delta\lambda=\frac{an_3''+2\exp\left(-2\kappa_2 d_2\right)\sin 2\Phi_{12}\sin 2\Phi_{32}}{|\chi|} \tag{A20}$$

and on-resonance (i.e. maximum) value:

$$|t_{14}|_{\mathrm{res}}^2=\frac{64\exp\left(-2\kappa_2 d_2\right)\cos^2\Phi_{12}\sin^2\Phi_{32}\cos^2\Phi_{34}}{\left(an_3''+2\exp\left(-2\kappa_2 d_2\right)\sin 2\Phi_{12}\sin 2\Phi_{32}\right)^2}. \tag{A21}$$

*Calculation of* $|r_{14}|^2$. The reflection coefficient given in (16) can be expressed under the form:

$$r_{14} = \frac{r_{12}P + Q}{P + r_{12}Q} \tag{A22}$$

with

$$\begin{aligned} P &= r_{32} + r_{23}r_{32}r_{34}\exp(2\mathrm{i}k_{z3}d_3) \\ Q &= (r_{23}r_{32} + r_{32}r_{34}\exp(2\mathrm{i}k_{z3}d_3))\exp(-2\kappa_2 d_2)\,. \end{aligned} \tag{A23}$$

Let us write out the terms $P$ and $Q$. Expanding their expressions in $n_3''$, $\exp(-2\kappa_2 d_2)$, and $\Psi$, and retaining only the lowest-order terms, we find

$$\mathrm{P} \approx r_{32} + r_{23}\left(1 - an_3'' + \mathrm{i}\Psi\right) = r_{32}\left(an_3'' - \mathrm{i}\Psi\right) \tag{A24}$$

and

$$Q \approx r_{32}\left[r_{23} + \frac{1}{r_{32}}\left(1 - an_3'' + \mathrm{i}\Psi\right)\right]\exp(-2\kappa_2 d_2)\,. \tag{A25}$$

Because of the term $\exp(-2\kappa_2 d_2)$ in expression (A25), we can neglect the terms in $n_3''$ and $\Psi$ inside the brackets:

$$Q \approx r_{32}\left[-r_{32} + \frac{1}{r_{32}}\right]\exp(-2\kappa_2 d_2) \approx 2\mathrm{i}r_{32}\sin 2\Phi_{32}\exp(-2\kappa_2 d_2)\,. \tag{A26}$$

Replacing $P$ and $Q$ in (A22), we obtain

$$r_{14} \approx r_{12}\frac{an_3'' - \mathrm{i}\Psi + (2\mathrm{i}/r_{12})\sin 2\Phi_{32}\exp(-2\kappa_2 d_2)}{an_3'' - \mathrm{i}\Psi + 2\mathrm{i}r_{12}\sin 2\Phi_{32}\exp(-2\kappa_2 d_2)}\,. \tag{A27}$$

Because of the total reflection at the prism–gap interface, we have $1/r_{12} = \exp(2\mathrm{i}\Phi_{12})$, and hence

$$r_{14} \approx r_{12}\frac{an_3'' - 2\sin 2\Phi_{12}\sin 2\Phi_{32}\exp(-2\kappa_2 d_2) + \mathrm{i}\,(2\cos 2\Phi_{12}\sin 2\Phi_{32}\exp(-2\kappa_2 d_2) - \Psi)}{an_3'' + 2\sin 2\Phi_{12}\sin 2\Phi_{32}\exp(-2\kappa_2 d_2) + \mathrm{i}\,(2\cos 2\Phi_{12}\sin 2\Phi_{32}\exp(-2\kappa_2 d_2) - \Psi)}\,. \tag{A28}$$

Taking the squared modulus of this expression, we finally obtain:

$$|r_{14}|^2 \approx 1 - \left(1 - |r_{14}|^2_{\mathrm{res}}\right)\frac{\Delta\lambda^2}{(\lambda - \lambda_{\mathrm{res}})^2 + \Delta\lambda^2} \tag{A29}$$

with

$$|r_{14}|^2_{\mathrm{res}} = \frac{\left(an_3'' - 2\sin 2\Phi_{12}\sin 2\Phi_{32}\exp(-2\kappa_2 d_2)\right)^2}{\left(an_3'' + 2\sin 2\Phi_{12}\sin 2\Phi_{32}\exp(-2\kappa_2 d_2)\right)^2}\,. \tag{A30}$$

## References


[1] Cook R J and Hill R K 1982 *Opt. Commun.* **43** 258

[2] Balykin V I, Letokhov V S, Ovchinnikov Yu B and Sidorov A I 1987 *JETP Lett.* **45** 353; 1988 *Phys. Rev. Lett.* **60** 2137

[3] Hajnal J, Baldwin K, Fisk P, Bachor H and Opat G 1989 *Opt. Commun.* **73** 331

[4] Kasevich M, Weiss D and Chu S 1990 *Opt. Commun.* **15** 607

[5] Helmerson K, Rolston S L, Goldner L and Phillips W D 1992 *Optics and Interferometry with Atoms*, *WE-Heraeus-Seminar (Konstanz)*, Abstracts (unpublished)

[6] Aminoff C, Steane A, Bouyer P, Desbiolles P, Dalibard J and Cohen-Tannoudji C 1993 *Phys. Rev. Lett.* **71** 3083

[7] Esslinger T, Weidemüller M, Hemmerich A and Hänsch T W 1993 *Opt. Lett.* **18** 450

[8] Feron S *et al* 1993 *Opt. Commun.* **102** 83
[9] Seifert W, Adams C, Balykin V, Heine C, Ovchinnikov Y and Mlynek J 1994 *Phys. Rev.* A **49** 3814
[10] Seifert W, Kaiser R, Aspect A and Mlynek J 1994 *Opt. Commun.* **111** 566
[11] Aspect A, Henkel C, Labeyrie G and Landragin A 1995 *Proc. Int. School of Physics Enrico Fermi, Course CXXXI* (to be published)
[12] Kaiser R, Labeyrie G, Landragin A, Vansteenkiste N, Westbrook C I, Von Zanthier J and Aspect A 1995 *Proc. Int. Conf. on Laser Physics* (*Laser Phys.* to appear)
[13] Nesnidal R and Walker T 1996 *Appl. Opt.* submitted
[14] Kaiser R, Lévy Y, Vansteenkiste N, Aspect A, Seifert W, Leipold D and Mlynek J 1994 *Opt. Commun.* **104** 234
[15] This method of analysis is an extension of that followed in Ulrich R 1970 *J. Opt. Soc. Am.* **60** 1337, where we add the effect of the losses.
[16] Born M and Wolf E 1959 *Principles of Optics* (Oxford: Pergamon)
[17] Direct probing of the amplitude of the evanescent wave has been performed using the tip of an optical fibre. See for instance: Bielfeldt H, Hecht B, Herminghaus S, Mlynek J and Marti O 1993 *Near Field Opt.* **281**
Knight J C, Dubreuil N, Sandoghar V, Hare J, Lefèvre-Seguin V, Raimond J M and Haroche S 1995 *Opt. Lett.* **20** 1515
[18] Lévy Y 1972 *Nouv. Rev. Opt. Appl.* **3** 25
[19] For the principle of the shear-plate interferometer, see for instance Murty M V R K 1964 *Appl. Opt.* **3** 531
[20] Tien P K and Ulrich R 1970 *J. Opt. Soc. Am.* **60** 1325